CRYSTAL GROWTH & DESIGN

Article

pubs.acs.org/crystal

Measurement of Polar Plots of Crystal Dissolution Rates Using Hot-Stage Microscopy. Some Further Insights into Dissolution Morphologies

Meenesh R. Singh,[†,§] Nandkishor Nere,[‡] Hsien-Hsin Tung,[†,‡] Samrat Mukherjee,[‡] Shailendra Bordawekar,[‡] and Doraiswami Ramkrishna*[,†]

[†]School of Chemical Engineering, Purdue University, West Lafayette, Indiana, United States

[‡]Process Engineering & Sciences, GPRD - Process R&D, AbbVie Inc., North Chicago, Illinois, United States

[§]Joint Center for Artificial Photosynthesis, Lawrence Berkeley National Laboratory, Berkeley, California, United States

ABSTRACT: Polar plots are the representations of anisotropic surface properties such as surface energies and growth rates of crystalline materials. The steady-state morphologies of growing crystals are usually obtained from Wulff constructions on the polar plots of growth rates, whereas the morphologies of dissolving crystals are known to have no steady states. Here we show that the dissolving crystal can attain steady-state morphologies under certain conditions. The Wulff construction on the polar plots of dissolution time (or slowness) can be used to identify such steady-state morphologies. It is shown that the dissolving crystal can attain faceted morphology composed of fast dissolving faces. The evolution of dissolving crystals toward faceted morphology involves disappearance of slow-dissolving faces, which also causes vanishing of curvatures from the crystal surface. This article presents a method to experimentally determine polar plots from the dynamic images of crystals obtained from hot-stage microscopy. The method relies on the solution of the characteristics for crystal dissolution. The methodology is demonstrated to obtain polar plots of succinic acid at different subsaturations.

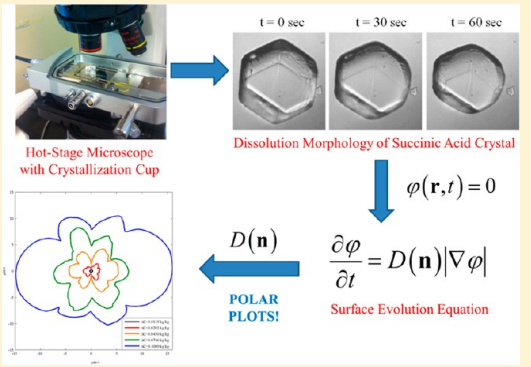

1. INTRODUCTION

Crystalline materials are known to have anisotropic surface properties due to the presence of face-specific molecular arrangements. These molecular arrangements stem from the crystal structure and possess symmetry that allows a group of faces, known as family, to share identical arrangements. The commonly observed anisotropic surface properties such as surface energies, growth rates, dissolution rates, wettability, cohesion, and adhesion can be expressed using polar plots. The polar plots of anisotropic surface properties of crystalline materials are the closed surfaces, where each point on the surface is the *property vector* in the direction of the normals of crystal faces.[1] The polar plots can be expressed as

$$P = f(\mathbf{n}) \tag{1}$$

where P can be any surface property and f is the scalar function of face-specific normals $\mathbf{n}$. One of the earliest applications of polar plots of surface energies can be found in the development of *Wulff construction*[2] which provides solution to the Gibbs' formulation of equilibrium crystal morphology.[3] The Wulff construction results from Wulff's theorem which was formally proved by Taylor,[4] showing that for any function f of surface normals there is a convex morphology which has the least surface integral for a fixed volume. If $f(\mathbf{n})$ represents the polar plot of surface energies, then the convex morphology is the equilibrium crystal morphology whose faces correspond to the location of cusps in the polar plots. As the crystals grow far from equilibrium, their morphologies are determined by the growth rates. According to Hartman-Perdok theory,[5−7] the polar plots of growth rates are proportional to that of surface energies and have similar features. The surface evolution equation describes the dynamics of crystal morphology for a given polar plot of growth rates. The characteristics of such equations produce shocks and fans, which indicate faceted evolution of crystal morphology toward the steady state, which can also be predicted from the Wulff construction on the polar plot of growth rates.[8,9] The usage of polar plots are not only limited to determining morphologies but can also be extended to designing crystals of enhanced properties such as low wettability, high dissolution rates, less cohesive, etc. The identification of polar plots can help in predetermining properties of crystals.

The kinematic theory of crystal dissolution and growth was initially proposed by Frank,[10] who extended the approach of Lighthill and Whitham[11,12] to the flow of steps on crystal surfaces. Frank's analysis yielded the dissolution polar plots from solution of kinematic wave equation which was based on

Received: June 27, 2014
Revised: September 24, 2014
Published: September 26, 2014

   dx.doi.org/10.1021/cg500939t | *Cryst. Growth Des.* 2014, 14, 5647−5661

the postulate that the flux of steps on the crystal surface is proportional to the local density of steps. His theory was based on microscopic details of crystal surface, which may not be always accessible, to predict surface evolution. Alternatively, the theory of Lacmann, Franke, and Heimann[13] uses the polar plots of dissolution rates to determine dissolution shapes, which is the solution of surface evolution equation. They deduce that the dissolution morphologies (i) will eventually have faces of same family, (ii) may have curved or planar surfaces, and (iii) can be derived by "cutting off" the corners of equilibrium morphologies. These conclusions are valid for cubic crystals and may not extend to other crystal structures. Section 2.3 shows that the dissolution morphologies may contain more than one family of faces which may not be derivable by "cutting off" the corners of equilibrium morphologies. The analysis of dissolution shapes is particularly important in anisotropic etching of semiconductors. Shaw[14] reported the localized etching profiles for different geometries and orientations of crystals from the polar plots of etch rates. Tellier and co-workers[15,16] obtained the analytical expressions of the dissolution slowness surfaces, which are the polar plots of dissolution time, for cubic crystals using the tensorial approach to the orientation-dependent etching process. One of the common observations by these researchers is that the dissolving crystal takes faceted morphology which can be determined from the extrema of the polar plots of dissolution rates and are also confirmed by the experiments.[17,18]

Doherty and co-workers[19−21] studied the dynamics of crystal morphology under small subsaturations. Their algorithm considers a finite number of faces that belongs to three categories such as (i) faces already present on crystal, (ii) F-faces, and (iii) the faces that are on vertices and edges formed by F-faces. The third category contains the fastest dissolving faces and does not involve the other fast dissolving faces that may contribute to the formation of curved interfaces. This approximation is subjected to the values of relative dissolution rates of other fast dissolving faces with respect to the fastest ones. Furthermore, the locations of fastest faces corresponding to the maxima of the polar plots may not lie exactly in between the adjacent F-faces. If there are dips (local minima) in the polar plots due to the presence of S-faces between the adjacent F-faces then there could be more than one face between the adjacent F-faces that can dominate the dissolution morphology. Considering the complexity of determining maxima of the polar plots, it is reasonable to assume that the fastest dissolving faces are equiangular from the adjacent F-faces. Moreover, they concluded that "in dissolution, crystals evolve away from the unique steady-state".[19] However, in some cases stable steady states can be realized as shown in their own simulation results. Similar results of computational etching profiles presented by other authors that show the existence of steady-state morphologies.[13,15]

The objectives of this article are (i) to develop dynamic equations for crystal morphology evolution during dissolution and determine the criteria to obtain steady-state morphologies and (ii) to develop methodology to obtain polar plots of dissolution rates from dynamics images of crystals. Section 2 discusses the surface evolution equations for dissolving crystals, presents the conditions for the existence of steady-state dissolution morphologies that could be either faceted or curved, and develops kinetic equations for the dissolution morphology of single crystal. Section 3 introduces our methodology to obtain polar plots of dissolution rates from the characteristics of surface evolution equations using the crystal images. Successively, it introduces a method to treat the experimentally obtained polar plots using crystal symmetry. Section 4 details the experimental methods for obtaining dynamic images of crystals using hot-stage microscopy. Section 5 implements the methodology to experimentally determine the polar plots of dissolution rates of succinic acid at different subsaturations and obtains the kinetic parameters for the shape evolution model. Section 6 provides the conclusions and future outlook.

2. MODELING OF GROWTH AND DISSOLUTION

The retreating or progressing crystal surfaces during dissolution or growth can be described by surface evolution equations of Jacobi-Hamilton type. One of the popular techniques to solve such equations is the Level Set Method.[22] These equations are amenable to the solution by Method of Characteristics.[8,9] The appearances of fans and shocks in the characteristics often result in the faceted evolution of crystal morphologies during growth or dissolution, which may under certain conditions attain a steady state. The subsequent sections develop necessary equations for morphology evolution during crystal dissolution.

2.1. Surface Evolution Equation. The growth/dissolution of crystals can be described by the progressing/receding surface, $\varphi(\mathbf{r};t) = 0$, due to the normal growth/dissolution rates that are functions of surface normals alone. The evolution of the surface under dissolution can be described by the following first-order partial differential equation,

$$\frac{\partial}{\partial t}\varphi(\mathbf{r};\, t) - \mathbf{D}(\mathbf{n})\cdot\nabla\varphi(\mathbf{r};\, t) = 0 \tag{2}$$

where $\mathbf{D}(\mathbf{n})$ is the dissolution rate as a function of the surface normal $\mathbf{n} = \nabla\varphi/\|\nabla\varphi\|$ and $\mathbf{r}$ is the position vector. The solution of eq 2 can be obtained by the Method of Characteristics.[23] The solution is given by

$$\varphi(\mathbf{r},\, t) = \varphi_0(\mathbf{r}(t)) \tag{3}$$

along the characteristics

$$\frac{\mathrm{d}\mathbf{r}}{\mathrm{d}t} = -D(\mathbf{n})\mathbf{n} - \left(\frac{\partial D}{\partial\theta}\right)_{\max}\mathbf{T} \tag{4}$$

such that

$$\frac{\mathrm{d}\mathbf{n}}{\mathrm{d}t} = \mathbf{0} \tag{5}$$

where $\mathrm{d}\theta$ is the magnitude of angular change in $\mathbf{n}$ and $\mathbf{T}$ is the tangent vector to the crystal surface in the direction of maximum increase in D with $\mathbf{n}$. Since the dissolution rates are described along the surface normals, they can be written as $\mathbf{D}(\mathbf{n}) \equiv D(\mathbf{n})\mathbf{n}$. The function $D(\mathbf{n})$ is popularly known as *polar plot* of dissolution rates. The normal component of the characteristics can be written as

$$\mathbf{n}\cdot\frac{\mathrm{d}\mathbf{r}}{\mathrm{d}t} = -D(\mathbf{n}) \tag{6}$$

The characteristics $\mathbf{r}(t)$ will evolve along the direction of the surface normal $\mathbf{n}$ such that $D(\mathbf{n})$ remain invariant in time. The characteristics for the crystal growth can be obtained by replacing $-D(\mathbf{n})$ with $G(\mathbf{n})$ such that

$$\mathbf{n}\cdot\frac{d\mathbf{r}}{dt} = G(\mathbf{n}) \tag{7}$$

dx.doi.org/10.1021/cg500939t | Cryst. Growth Des. 2014, 14, 5647−5661

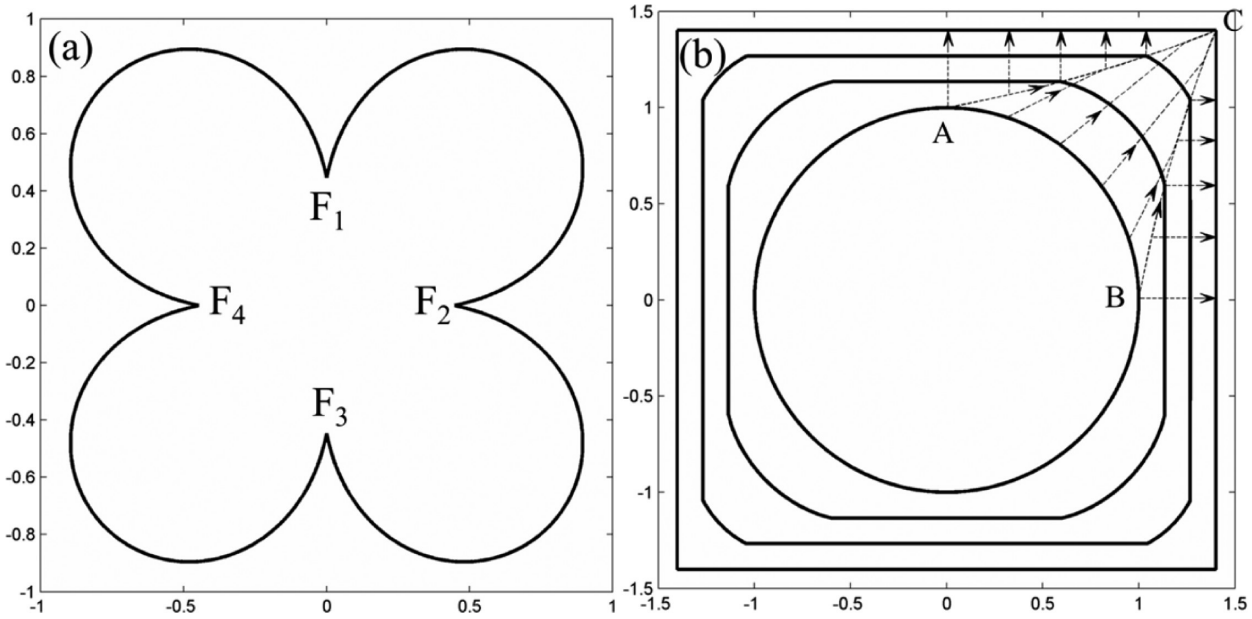

Figure 1. (a) Polar plot of growth rates limited by surface integration. The minima F_1, F_2, F_3, and F_4 of the polar plot correspond to the F-faces. (b) Evolution of a circular crystal to a square shape is governed by the characteristics shown as dotted arrows. The shocks are propagating along $\overrightarrow{AC}$ and $\overrightarrow{BC}$ and finally merging at *C*. The fans are appearing along the normals of F-faces.

The dissolution 6 and growth 7 characteristics are very well studied in the literature and are known to produce shocks and fans to give them faceted morphologies. The shocks are produced when multiple characteristics intersect, and fans appear when characteristics run parallel to each other. The identification of shocks and fans is relatively straightforward for planar crystals because of the absence of saddle points on the planar polar plots which, on the other hand, may be present on 3D polar plots. In the next section, we will explore the behavior of growth and dissolution characteristics under different limiting conditions of surface integration, surface diffusion, and bulk diffusion to assess the steady-state shapes of crystals.

2.2. Growth and Dissolution Morphologies: Faceted or Curved? During crystal growth, solute molecules move from the bulk solution to the crystal surface (bulk diffusion) followed by their transfer along the surface to the kink sites (surface diffusion), where they attach to the surface (surface integration). The process of dissolution is exactly the reverse of growth, where the molecules are transferred from the crystal surface to the bulk solution by a series of operations involving surface disintegration, surface diffusion, and bulk diffusion. If the solute transfer is limited by any of the foregoing processes such as surface integration/disintegration, surface diffusion, and bulk diffusion then the growth/dissolution rates of crystal faces will become dependent on their surface energies (specifically, the attachment energies), surface diffusivities, and bulk diffusivity, respectively.

2.2.1. Growth Morphologies. In the case of surface integration limited growth, the polar plot of growth rates (shown in Figure 1a) is proportional to that of attachment energies. The polar plots have cusps at their minima which usually correspond to the F-faces (flat faces). The F-faces are the crystal faces with more than one periodic bond chain that makes them stable (low energy) and slow growing as compared to the other faces. Figure 1a corresponds to the crystal of 4-fold symmetry with four F-faces located at F_1, F_2, F_3, and F_4. The specific polar function used in plotting Figure 1a is

$$G(\mathbf{n}) = \sqrt{|\sin[2\tan^{-1}(n_y/n_x)]| + 0.2} \tag{8}$$

where n_x and n_y are the x and y components of the surface normal $\mathbf{n}$. The faces in between the F-faces are of high energies and may correspond to either S-faces (step faces) or K-faces (kink faces). The Wulff construction in Figure 1a will determine the steady-state morphology, which is of square shape. Figure 1b shows the evolution of a circular crystal determined by the growth characteristics 7 emanating from the surface. As the crystal in this example has 4-fold symmetry, the characteristics shown as dotted arrows in Figure 1b behave identically in each quadrant.

The propagating shocks $\overrightarrow{AC}$ and $\overrightarrow{BC}$ are the sources for the fans (horizontal and vertical characteristics that run parallel to each other) appearing in Figure 1b. The propagating shocks are also the trajectories of the singular points on the crystal. The characteristics corresponding to surface normals in between $\mathbf{n}_1 = [0 \quad 1]^T$ and $\mathbf{n}_2 = [1 \quad 0]^T$ converges gradually to the propagating shocks which then merge at *C*. A characteristic will converge to the propagating shocks if the corresponding normal satisfies the following relationship

$$G(\mathbf{n}) > \mathbf{n}^T \begin{bmatrix} \mathbf{n}_1^T \\ \mathbf{n}_2^T \end{bmatrix}^{-1} \begin{bmatrix} G(\mathbf{n}_1) \\ G(\mathbf{n}_2) \end{bmatrix} \tag{9}$$

Here $\mathbf{n}_1$ and $\mathbf{n}_2$ are the face normals corresponding to the adjacent minima of the planar polar plot. The time of intersection of the characteristics with the propagating shocks depends on the initial shape of the crystal. The fans are located at normal vectors which minimizes the polar plot such that

$$\min_n G(\mathbf{n}) \tag{10}$$

Therefore, the growth of any arbitrary-shaped crystal, governed by the surface integration limited growth rates, will take a faceted morphology with a discrete number of fans forming flat

dx.doi.org/10.1021/cg500939t | *Cryst. Growth Des.* 2014, 14, 5647−5661

faces whose normals correspond to the cusps of the governing polar plot. A set of characteristics 7 associated with the ith fan can be lumped into a single ordinary differential equation (ODE), such that

$$\mathbf{n}_i \frac{d\mathbf{r}}{dt} = \frac{d\tilde{h}_i}{dt} = G(\mathbf{n}_i),\ i = 1, 2, ..., n \tag{11}$$

Here $\tilde{h}_i$ is the perpendicular distance of a crystal face formed by the ith fan given as $\mathbf{n}_i \cdot \mathbf{r} = h_i$ and there are a total n such faces. The symmetry of the crystal allows faces with identical atomic arrangements, known as a family, to have same growth rates. Therefore, eq 11 can be further lumped into ODEs corresponding to each family of faces.

$$\frac{dh_i}{dt} = G_i,\ i = 1, 2, ..., m \tag{12}$$

where h_i represents perpendicular distances of faces in the ith family whose growth rates are $G_i = G(\mathbf{n}_i)$ and m is the total number of families. Equation 12 is sometimes referred to as the *shape evolution model*, which arises from the governing surface evolution equation. Equation 12 can be written in vector notations as

$$\frac{d\mathbf{h}}{dt} = \mathbf{G}(\mathbf{c}) \tag{13}$$

where $\mathbf{h}$ is an m-dimensional vector (also referred to as *h-vector*) of perpendicular distances and $\mathbf{G}$ is the vector of corresponding growth rates which can be a function of crystallization conditions $\mathbf{c}$. Equation 13 dictates the dynamics of F-faces (fans) that can lead to various morphology transformations due to the appearance or disappearance of faces governed by their relative growth rates. Singh et al.[24] developed a framework to identify the morphology domain that can elucidate all possible morphology transformations for any crystalline material. Furthermore, they developed dynamic equations for evolution of single crystal morphology and morphology distributions. Although $\mathbf{h}$ can never attain a steady state, the crystal morphology which is governed by the relative perpendicular distances can attain a steady-state when grown at fixed growth rates. The solution of 13 for fixed growth rates $\mathbf{G}$ is given as

$$\mathbf{h}(t) = \mathbf{h}(0) + \mathbf{G}t \tag{14}$$

After a sufficiently long time when $\|\mathbf{h}(t)\| \gg \|\mathbf{h}(0)\|$, the h-vector $\mathbf{h}$ will orient itself asymptotically along $\mathbf{G}$ such that

$$\mathbf{h} \propto \mathbf{G} \tag{15}$$

which is the required condition for steady-state morphology. Thus, a crystal can always attain steady-state morphology at fixed growth rates by growing sufficiently larger.

The growth of crystals is dominated by slow-growing faces whose vertices and edges are the regions of higher surface energies where all other fast-growing faces are located. Since the normal growth rates of crystal planes at vertices and edges of crystals are much higher, they tend to suffer with diffusion limitations. The growth in such situations for some portions of the crystal surface is regulated by surface integration, while the other portions evolve in diffusion controlled regime. The diffusion limitations may arise from either (i) surface diffusion or (ii) bulk diffusion. Since surface diffusivities are face specific, the corresponding polar plots of growth rates will have nonconstant curvature, whereas the polar plots limited by bulk diffusion have constant curvature. Figure 2a shows an example of a polar plot of growth rates where F-face are governed by surface integration, and all other faces are limited by surface diffusion. If the growth of the crystal is limited entirely by surface diffusion, the corresponding polar plots can take any smooth and closed shape. The specific polar function used to generate the polar plot in Figure 2a is

$$G(\mathbf{n}) = \sqrt{0.8|\sin[2\tan^{-1}(n_y/n_x)]| + 0.2} \tag{16}$$

The evolution of circular crystal directed by the growth rates 16 attains a steady-state nonfaceted morphology. The characteristics emanating vertically $\mathbf{n} = [0\ \ 1]^T$ and horizontally $\mathbf{n} = [1\ \ 0]^T$ from the circle produces fans (flat surfaces), and the characteristics corresponding to the faster growing faces diverge radially to yield curvature.

Figure 2c shows an example of the polar plots of growth rates of faces, whose normals make angles between 30° and 60°, driven by bulk diffusion. The polar function used in Figure 2c is given by

$$\begin{aligned} G(\mathbf{n}) &= \sqrt{0.8|\sin[2\tan^{-1}(n_y/n_x)]| + 0.2} \\ 0 \le \tan^{-1}(n_y/n_x) < 30,\ 60 < \tan^{-1}(n_y/n_x) \le 90 \\ &= \sqrt{0.8|\sin[2 \times 30]| + 0.2} \\ 30 \le \tan^{-1}(n_y/n_x) \le 60 \end{aligned} \tag{17}$$

The evolution of circular crystal in Figure 2d under the growth field 17 shows a similar behavior as in Figure 2b except that it takes a constant curvature for the portion influenced by the bulk diffusion. In both cases where crystal is partly governed by surface integration and partly by diffusion, the characteristics evolve into three groups producing (i) fans (normals satisfying eq 10), (ii) shocks (normals satisfying eq 9), and (iii) curvatures (rest of the normals).

The polar plots of growth rates limited by bulk diffusion will be a circle in two dimensions (shown in Figure 3a) and a sphere in three dimensions. The dynamics of the crystal shape in Figure 3b for the isotropic growth rates in Figure 3a shows radially emerging characteristics with no occurrences of shocks and fans. Therefore, a crystal growing under bulk diffusion limitation will eventually take a spherical shape.

2.2.2. Dissolution Morphologies. The process of dissolution of crystal is exactly the reverse of growth. The dynamics of crystal morphology during dissolution is determined by either the surface evolution eq 2 or the associated characteristics 6. The dissolving crystal can take either faceted or nonfaceted morphology based on the shape of polar plots which is governed by different controlling mechanisms such as surface disintegration, surface diffusion, and bulk diffusion. As opposed to the growth morphologies which are dominated by low energy faces, the dissolution morphologies are governed by high energy faces. The steady-state dissolution morphology can be determined from Wulff construction of the *Slowness Surface* of dissolution rates. The slowness surface $\tau(\mathbf{n})$ is defined as the inverse of the polar function of dissolution rates, such that

$$\tau(\mathbf{n}) = \frac{1}{D(\mathbf{n})} \tag{18}$$

Unlike crystal growth where steady-state morphologies can always be attained under fixed growth rates, the dissolution

dx.doi.org/10.1021/cg500939t | Cryst. Growth Des. 2014, 14, 5647−5661

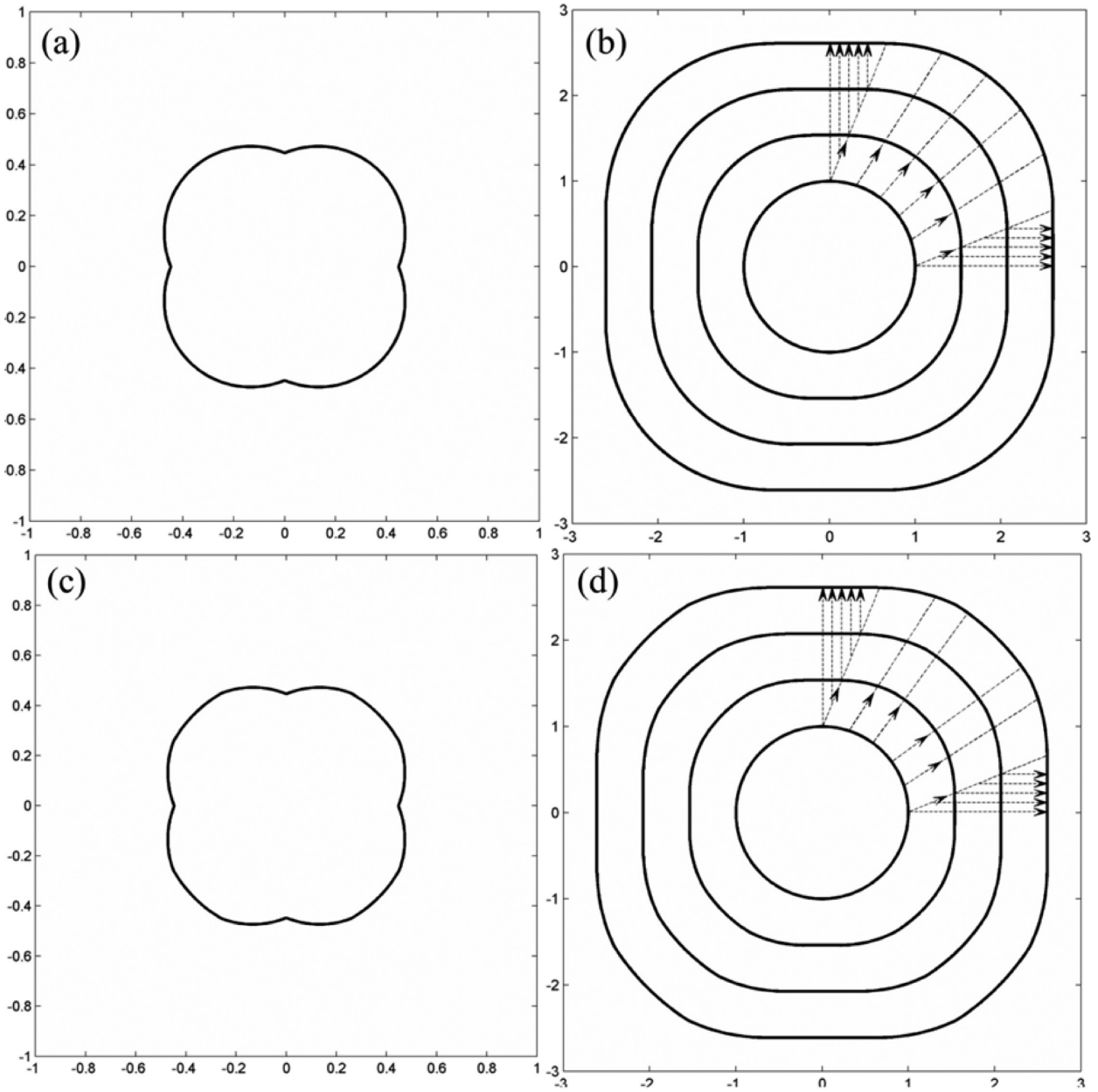

Figure 2. Polar plot of growth rates when the growth of F-faces are governed by surface integration and rest of the other faces are limited by (a) surface diffusion or (c) bulk diffusion. The evolution of circular crystals shown in (b) and (d) are dictated by the growth rates in (a) and (c), respectively. Panels (b) and (d) show the characteristics (dotted arrows) producing fans, shocks, and curvatures.

morphologies can attain steady state only under certain circumstances to be discussed in Section 2.3. The effect of different governing mechanisms such as surface disintegration, surface diffusion, and bulk diffusion on the dynamics of dissolution morphologies will be discussed next in terms of characteristics forming fans, shocks, and curvatures. The functional forms for the polar plots of dissolution rates in the subsequent analysis are chosen similar to those used for the growth rates in 8, 16, and 17, for comparison between growth and dissolution morphologies under similar conditions.

The dissolution of crystals controlled by surface disintegration is dependent on the detachment energies of solute molecules which is same as the attachment energies. The corresponding polar function of dissolution rates is given as

$$D(\mathbf{n}) = \sqrt{|\sin[2\tan^{-1}(n_y/n_x)]| + 0.2} \qquad (19)$$

Figure 4a shows the slowness surface 18 for the polar function 19 of dissolution rates. The minima of the slowness surface (equivalently, the maxima of the polar plot) indicated as K_1, K_2, K_3, and K_4 correspond to the faces of highest dissolution rates. These faces are also the highest energy faces and may belong to K-faces. The Wulff construction in Figure 4a suggests steady-state morphology of diamond shape. Figure 4b shows the evolution of circular crystal to a diamond shape. The characteristics are progressing inwardly from the initial surface and diverging away from the 45° line. Consequently, the shocks produced along $\overrightarrow{AC}$ and $\overrightarrow{BC}$ will create vertices on the crystal surface. The trajectories of shocks depend on the initial shape of the crystal whose location on the steady-state morphology can be determined from the positions of fans.

dx.doi.org/10.1021/cg500939t | Cryst. Growth Des. 2014, 14, 5647−5661

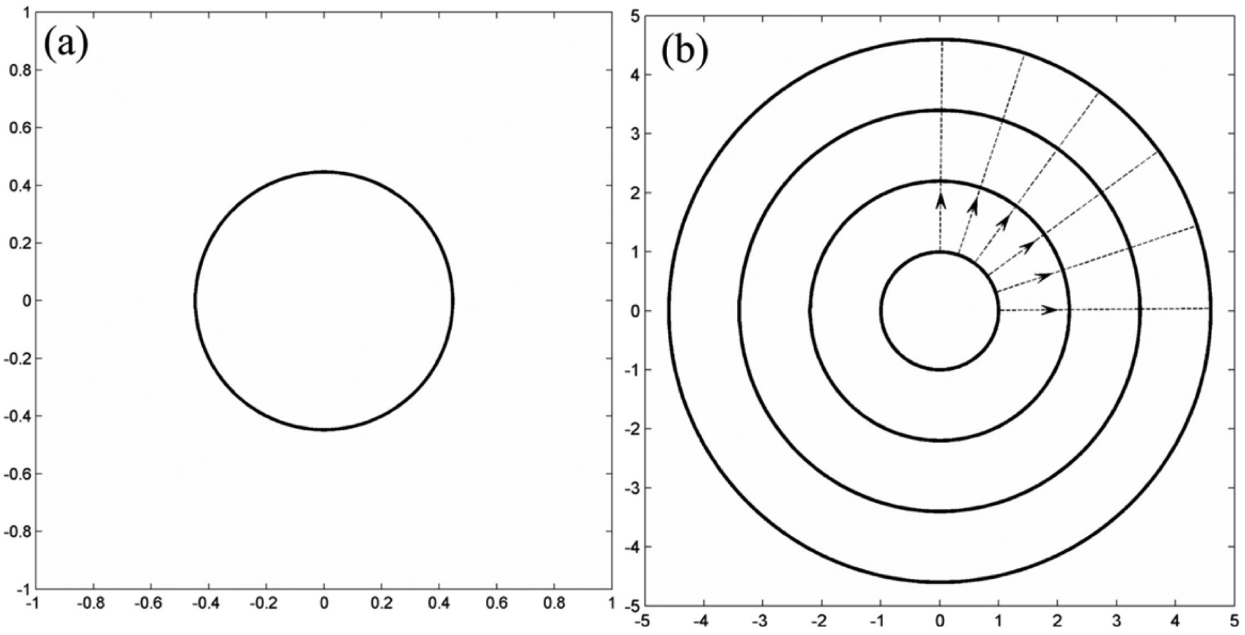

Figure 3. (a) Isotropic polar plot of growth rates when bulk diffusion is a controlling mechanism. (b) Invariant evolution of circular crystal where characteristics (dotted arrows) are neither creating shocks nor fans.

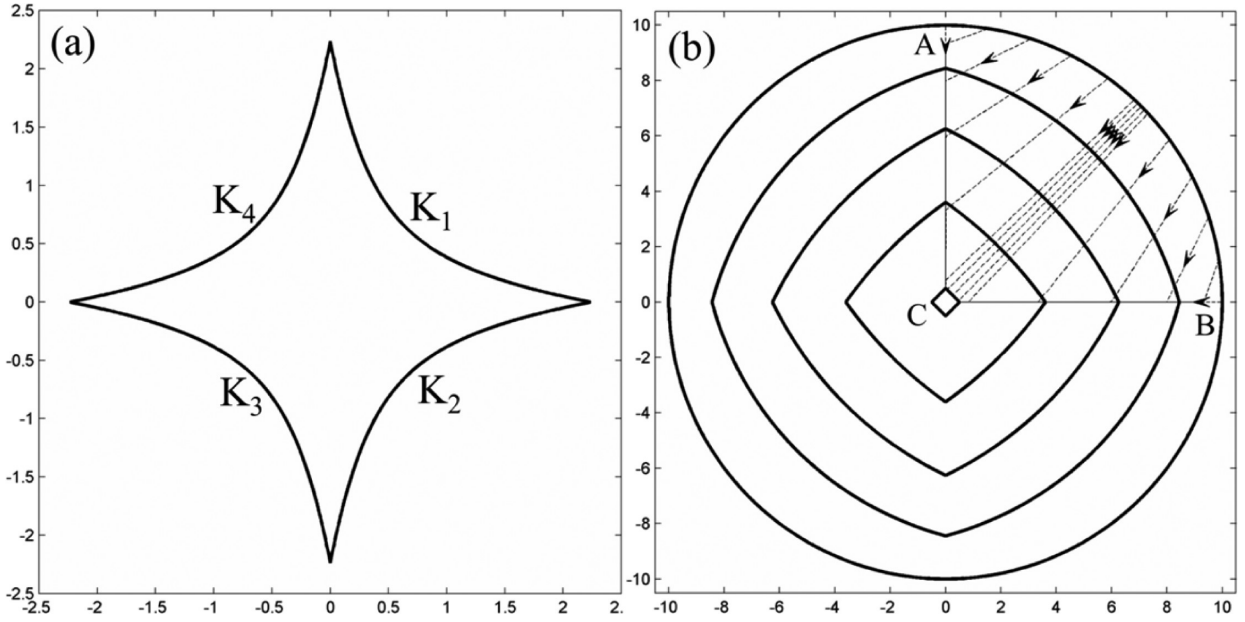

Figure 4. (a) Slowness surface for the polar plot of dissolution rates in Figure 1a. The minima of the slowness surface indicated as K_1, K_2, K_3, and K_4 are the K-faces of highest dissolution rates. (b) Dissolution of circular crystal to diamond shape governed by the slowness surface in (a). Characteristics shown as dotted arrows are diverging away from the 45° line and producing shocks along $\overrightarrow{AC}$ and $\overrightarrow{BC}$. Fans appear along the minima of the slowness surface.

The mechanism of the appearance of fans during dissolution is different than that of growth where fans appear from the propagating shocks. The characteristics emanating from a small patch on the initial surface nearthe 45° line in Figure 4b are less diverging and appear to be parallel. As the crystal dissolves, its surface becomes dominated by less diverging and almost parallel characteristics. The appearance of fans is therefore due to a decrease in crystal size and existence of a finite number of maxima in the polar plots of dissolution rates. The fans for dissolution morphologies are located at the surface normals that maximize the polar plots of dissolution rates, such that

$$\max_{\mathbf{n}} D(\mathbf{n}) \tag{20}$$

Usually there are only a finite number of normal vectors that will maximize the polar plot of dissolution rates. However, in some cases there could be infinite solutions to the maximization problem 20 which will be discussed subsequently. The characteristics producing shocks are those whose associated normals satisfy following condition

$$D(\mathbf{n}) < \mathbf{n}^T \begin{bmatrix} \mathbf{n}_1^T \\ \mathbf{n}_2^T \end{bmatrix}^{-1} \begin{bmatrix} D(\mathbf{n}_1) \\ D(\mathbf{n}_2) \end{bmatrix} \tag{21}$$

dx.doi.org/10.1021/cg500939t | Cryst. Growth Des. 2014, 14, 5647−5661

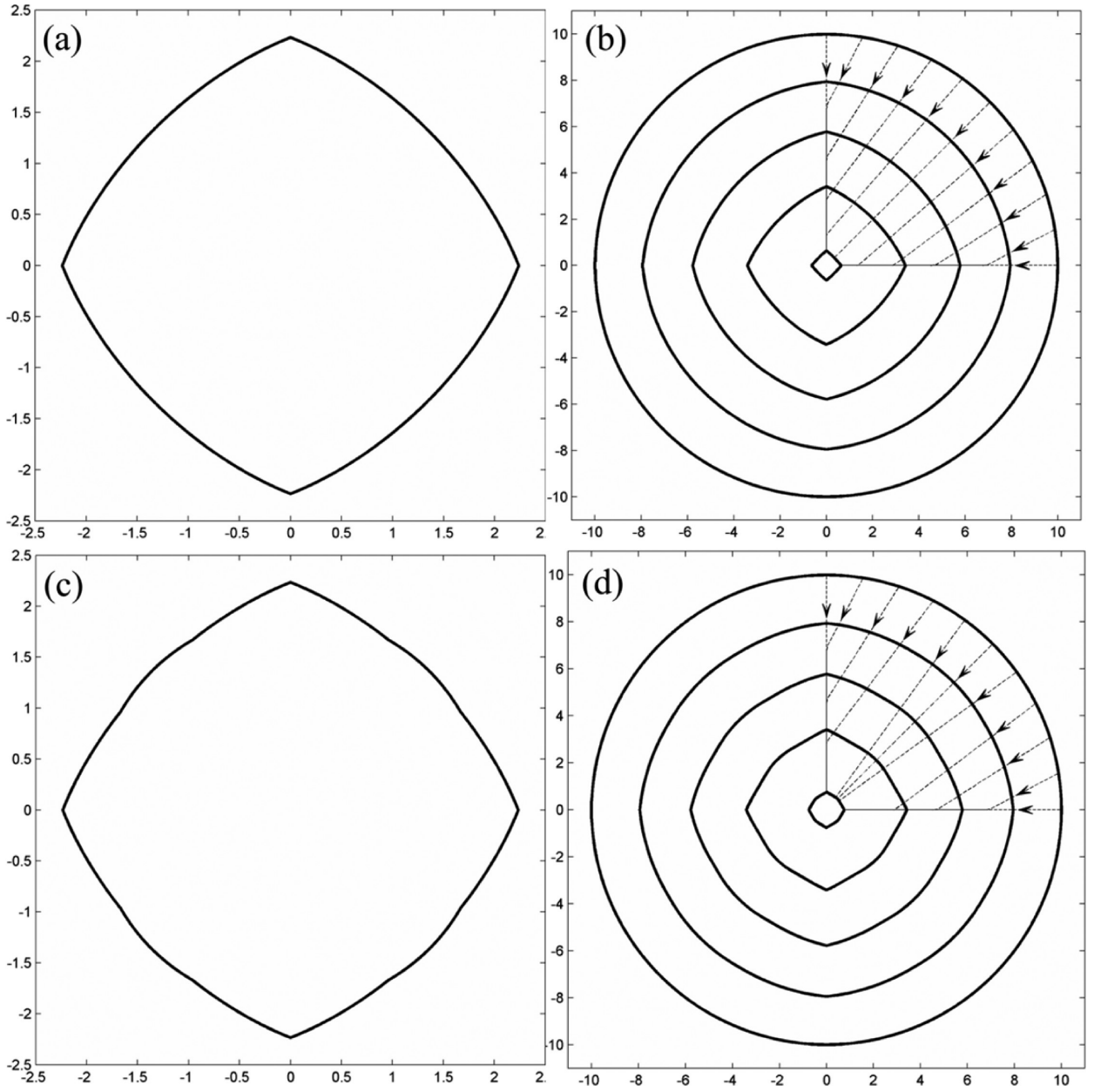

Figure 5. Slowness surface for dissolution rates when the dissolution of F-faces are governed by surface disintegration and rest other faces are limited by (a) surface diffusion or (c) bulk diffusion. The evolution of circular crystals shown in (b) and (d) are dictated by corresponding dissolution rates in (a) and (c), respectively. Panels (b) and (d) show the characteristics (dotted arrows) producing fans, shocks, and curvatures.

where $\mathbf{n}_1$ and $\mathbf{n}_2$ are the normal vectors adjacent to normal vectors satisfying eq 20. The normal vectors satisfying eq 21 will eventually intersect at the propagating shocks, which will reduce the curvature of the crystal surface and make it faceted. Therefore, the crystal dissolving via surface disintegration will take a shape composed of a finite number of highest energy faces. The evolution of such faceted morphology can be conveniently described as

$$\frac{d\mathbf{h}}{dt} = -\mathbf{D}(\mathbf{c}) \tag{22}$$

Here $\mathbf{h}$ and $\mathbf{D}$ are m-dimensional vectors of perpendicular distances of flat faces and their dissolution rates, respectively. Equation 22 can be obtained in a similar fashion as shown for growth in eqs 11−13. The vector of dissolution rates has components $D_i = D(\mathbf{n}_i)$ evaluated for the normal vector corresponding to the ith family of faces. The faceted evolution can lead to appearance of disappearance of faces which can be identified by constructing morphology domain. At fixed crystallization conditions, the solution of eq 22 can be obtained as

$$\mathbf{h}(t) = \mathbf{h}(0) - \mathbf{D}t \tag{23}$$

It can be shown by defining relative perpendicular distances that the dissolution morphology cannot attain steady state; in other words, $\mathbf{h}$ cannot be aligned to $\mathbf{D}$. However, under certain conditions the morphology may attain a steady state, which will be discussed in the next section.

Rates of the fastest dissolving faces are susceptible to diffusion limitations such that some parts of the crystal surface are controlled by diffusion and the rest by surface disintegration. Figure 5a shows the slowness surface for the polar function of dissolution rates

dx.doi.org/10.1021/cg500939t | Cryst. Growth Des. 2014, 14, 5647−5661

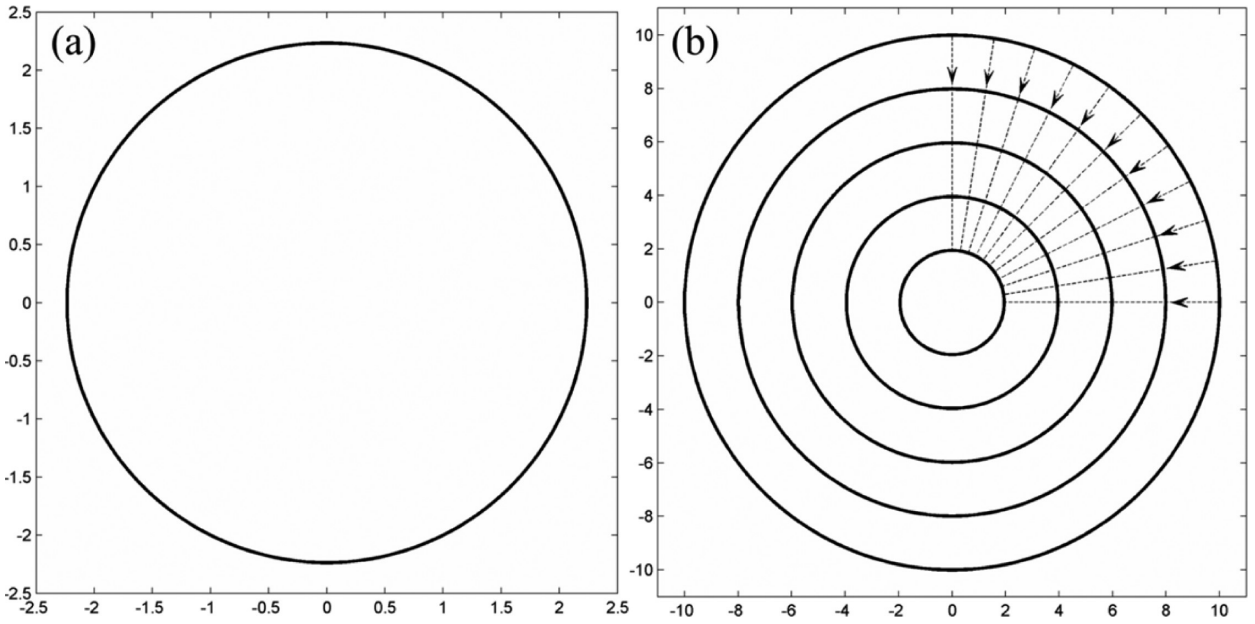

Figure 6. (a) Isotropic slowness surface for dissolution rates when bulk diffusion is a controlling mechanism. (b) Invariant evolution of circular crystal where characteristics (dotted arrows) are neither creating shocks nor fans.

$$D(\mathbf{n}) = \sqrt{0.8|\sin[2\tan^{-1}(n_y/n_x)]| + 0.2} \tag{24}$$

which are partially governed by surface diffusion. The polar plot of dissolution rates expressed by eq 24 is shown in Figure 2a. As the surface diffusivity is different for different faces, the curvature of slowness surface in Figure 5a varies with the surface normal which results in a finite number of maxima. Therefore, the Wulff construction on such slowness surface would yield faceted steady-state morphology. Figure 5b shows the evolution, governed by the dissolution rates in eq 24, of circular crystal to the diamond shape. The dynamical behavior of characteristics are similar to those in Figure 4b, the fans appear along $[1\ 1]^T$, $[-1\ 1]^T$, $[-1\ -1]^T$ and $[1\ -1]^T$ directions and the shocks move toward $[1\ 0]^T$, $[0\ 1]^T$, $[-1\ 0]^T$ and $[0\ -1]^T$ directions. The fans become more prominent as the crystal dissolves to a smaller size. Although the growth rates in eq 16 and dissolution rates in eq 24 share a similar form, the corresponding steady-state shape is curved (nonfaceted) for growth and faceted for dissolution.

The fast dissolving faces can also be limited by bulk diffusion resulting in identical dissolution rates. Figure 5c shows the slowness surface for the polar function of dissolutions rates

$$\begin{aligned} D(\mathbf{n}) &= \sqrt{0.8|\sin[2\tan^{-1}(n_y/n_x)]| + 0.2} \\ 0 \le \tan^{-1}(n_y/n_x) < 30,\ 60 < \tan^{-1}(n_y/n_x) \le 90 &= \sqrt{0.8|\sin[2\times 30]| + 0.2} \\ 30 \le \tan^{-1}(n_y/n_x) \le 60 & \end{aligned} \tag{25}$$

which are partially governed by bulk diffusion. The corresponding polar plot for eq 25 is shown in Figure 2c. As the bulk diffusivity is independent of crystal faces, the corresponding portion of the slowness surface will exhibit an infinite number of maxima and will have a constant curvature. The Wulff construction in Figure 5c will yield partially faceted steady-state morphology with curvatures of constant radius. Figure 5d shows the evolution of circular crystal to such a steady state. The shocks appear at the same locations as in Figures 4b and 5b. However, the fans are appearing along 30° and 60° lines whose locations are different than in Figures 4b and 5b. The characteristics corresponding to the normal vectors between 30° and 60° converges radially to produce a curvature of constant radius.

The polar plots of dissolution rates are smooth functions if the dissolution of entire crystal is controlled by diffusion. The polar plot and hence the slowness surface (shown in Figure 6a) are exactly circular if the dissolution is governed by bulk diffusion. Consequently, the dissolving crystal in Figure 6b attains circular steady-state morphology.

2.3. Conditions for Steady-State Dissolution Morphology. The Wulff construction on the slowness surface would yield steady-state dissolution morphology. However, such steady states can be only attained under certain circumstances. Figures 4b and 5b show the transformation of circular morphology (with all faces present) to a faceted morphology (with a few faces) in the absence of bulk diffusion limitations. In presence of bulk diffusion, the crystal can eventually develop curvatures of constant radius as shown in Figures 5d and 6b. These morphologies might undergo further transformations to achieve the steady state. Such transformations can be described by the evolution of shape determining variables such as perpendicular distances and radii of curvatures. Doherty and co-workers showed that the dissolution of faceted morphologies always move away from the corresponding steady state. Such evolution is described by the ODE 22 for perpendicular distances of each family of faces that are likely to appear. Depending on the relative dissolution rates, it is possible that some families of faces may disappear during evolution. If the ith family is disappearing on an already existing jth family on a crystal then the perpendicular distance h_i of the ith family becomes proportional to the perpendicular distance h_j of the jth family

$$h_i = \alpha_{ij} h_j \tag{26}$$

dx.doi.org/10.1021/cg500939t | Cryst. Growth Des. 2014, 14, 5647−5661

where α_{ij} is the proportionality constant. The dissolution rates of disappeared faces will also become dependent on the existing faces. Therefore, the dissolution rate of the ith family is related as

$$D_i = \alpha_{ij} D_j \tag{27}$$

Now consider a scenario when $(m-1)$ families of faces will gradually disappear and the crystal is left with only one family (say, the first family) of faces, such that

$$\mathbf{h} = h_1 \boldsymbol{\alpha} \tag{28}$$

where $\boldsymbol{\alpha} = [1 \quad \alpha_{21} \quad \dots \quad \alpha_{m1}]^T$. Similarly the vector of dissolution rates can be expressed as

$$\mathbf{D} = D_1 \boldsymbol{\alpha} \tag{29}$$

At fixed dissolution rates, the evolution of crystal morphology is given by eq 22 before attaining steady state. As all the families of faces disappear (except family 1), the dissolution rates become dependent and gradually take the form of eq 29. The morphology evolution is then described by $h_1(t)$. Since $\boldsymbol{\alpha}$ is independent of time, the vector of perpendicular distances will become parallel to the vector of dissolution rates when there is only one independent family of faces present on the crystal,

$$\mathbf{h}(t) \propto \mathbf{D} \tag{30}$$

As the relative perpendicular distances are proportional to relative dissolution rates, the crystal attains steady-state morphology. It is also possible that the crystal might completely disappear before attaining steady state.

The steady-state morphology determined from the Wulff construction on the slowness surface can have more than one family of faces. Their relative perpendicular distances will naturally move away from the steady state if they are not proportional to the corresponding relative dissolution rates. Therefore, the steady-state morphology with multiple families of faces can be attained if their relative perpendicular distances in the initial morphology are proportional to their relative dissolution rates.

2.4. Efficient Model for the Evolution of Nonfaceted or Smooth Morphologies. In the previous sections, we noticed that a crystal can undergo various transformations based on the governing mechanism to arrive at steady-state morphology. Although dissolution is described by a single surface evolution equation, its use is inconvenient for obtaining population trajectories. Therefore, the purpose of this section is to derive kinetic equations for shape-defining variables such as perpendicular distances and curvatures that can be used for efficient description of the population of crystals. Such models can be very useful to predict the evolution of crystal morphology distributions during cycles of growth and dissolution.

The Frenet equations for the planar curve can be used to derive kinetic equations for the change in curvature due to crystal growth or dissolution. From the Frenet equations, the curvature κ can be expressed as

$$\kappa = -\frac{\mathrm{d}\mathbf{n}}{\mathrm{d}s}\cdot\mathbf{T} \tag{31}$$

where s is the arc length whose differential element is $\mathrm{d}s = \|\mathrm{d}\mathbf{r}\|$. The rate of change in curvature can be obtained as

$$\frac{\mathrm{d}\kappa}{\mathrm{d}t} = \frac{\mathrm{d}\kappa}{\mathrm{d}s}\frac{\mathrm{d}s}{\mathrm{d}t} = -\left[\frac{\mathrm{d}^2\mathbf{n}}{\mathrm{d}s^2}\cdot\mathbf{T}\right]\frac{\mathrm{d}s}{\mathrm{d}t} \tag{32}$$

which can be further expressed in matrix notation as

$$\frac{\mathrm{d}\kappa}{\mathrm{d}t} = \mathbf{T}^T[\nabla(\nabla\mathbf{n}\mathbf{T})]\mathbf{T}\frac{\mathrm{d}s}{\mathrm{d}t} \tag{33}$$

The rate of change of arc length can be obtained from the characteristics as

$$\frac{\mathrm{d}s}{\mathrm{d}t} = \left[\frac{\mathrm{d}\mathbf{r}}{\mathrm{d}t}\cdot\frac{\mathrm{d}\mathbf{r}}{\mathrm{d}t}\right]^{1/2} = \left[v(\mathbf{n})^2 + \left(\frac{\mathrm{d}v}{\mathrm{d}\theta}\right)^2\right]^{1/2} \tag{34}$$

where $v(\mathbf{n})$ is equal to $G(\mathbf{n})$ for growth and $-D(\mathbf{n})$ for dissolution. Substituting eq 34 into 33 will remove the dependence of curvature on the arc length,

$$\frac{\mathrm{d}\kappa}{\mathrm{d}t} = \zeta(\varphi)\left[v(\mathbf{n})^2 + \left(\frac{\mathrm{d}v}{\mathrm{d}\theta}\right)^2\right]^{1/2} \tag{35}$$

where $\zeta(\varphi) = \mathbf{T}^T[\nabla(\nabla\mathbf{n}\,\mathbf{T})]\mathbf{T}$ is a scalar function involving up to third order derivatives of φ. The symmetry of crystals is usually reflected on the developed curvature which allows many characteristics to have identical curvature. The evolution of convex crystals with flat faces and curved interfaces can be completely described by eqs 13, 22, and 35.

The periodic operations of growth and dissolution are often used to manipulate crystal morphology. In doing so, the crystals can switch from the faceted growth morphology to the faceted dissolution morphology through a series of transformations involving the appearances of curved interfaces. For example, Figure 7 shows the dissolution of steady-state growth morphology (in Figure 1b) to steady-state dissolution morphology. The underlying polar plot of dissolution rates has the same shape as in Figure 1a. Notice that the initial morphology in Figure 7 is composed of slowest-dissolving faces

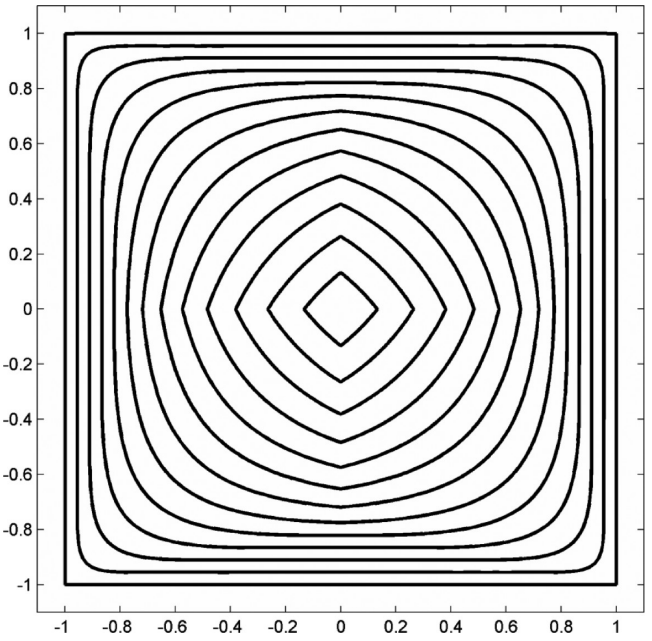

Figure 7. Dissolution of steady-state growth morphology (shown in Figure 1b) governed by the dissolution rates in eq 19.

dx.doi.org/10.1021/cg500939t | Cryst. Growth Des. 2014, 14, 5647−5661

which gradually disappear as the crystal recruits more fast-dissolving faces. Thus, the cyclic operation of growth and dissolution can help in manipulating not only morphology but also surface properties.

The initial morphology in Figure 7 has 4-fold symmetry and therefore requires only one perpendicular distance to determine the dynamics of the flat faces. Dissolution of the crystal results in the appearance of infinitely many faces forming a curved interface of constant curvature. Figure 8 shows the evolution of perpendicular distance, curvature, and the center of curvature for dissolving crystal in Figure 7.

The perpendicular distance follows a linear trajectory until the F-faces completely disappear, and then its evolution is dictated by the vertices formed by the faster dissolving faces. The evolution of the curvature from infinity to zero is a result of transition of the vertices (on initial morphology) to the flat faces (on final morphology). The center of curvature moves along the 45° line whose distance from the origin decreases with increase in time. Here the curvatures and their centers are determined by fitting an arc of a circle to the curved portion of the crystal. Initially, the evolution of dissolution morphology requires three internal coordinates such as perpendicular distance, curvature, and center of the curvature. After the disappearance of flat faces, the morphology can be described by only two internal coordinates such as curvature and its center. The evolution of morphology distributions can be described by population balance equations[25−27] with internal coordinates such as perpendicular distances (h), curvatures (κ), and corresponding centers of curvatures (r).

$$\frac{\partial n(h, \kappa, r; t)}{\partial t} - \frac{\partial}{\partial h} D(h, \mathbf{c})n - \frac{\partial}{\partial \kappa} K(\kappa, \mathbf{c})n - \frac{\partial}{\partial r} R(\kappa, r, \mathbf{c})n = 0 \tag{36}$$

The above equation describes the evolution of a population of nonfaceted crystals in subsaturated environment, where D is dissolution rate of faces with perpendicular distance h, K is the rate of change of curvature κ, and R is the rate of change of the center of curvature r. These rate kernels can be derived from the polar plots as follows. First, obtain the shape evolution of dissolving crystal using polar plots, as shown in Figure 7. Then, determine the time trajectories of curvature and its center by fitting circular arcs. And finally, cross plotting the derived rates $D(t)$ against $h(t)$; $K(t)$ against $\kappa(t)$; and $R(t)$ against $\kappa(t)$ will give the required kernels. Figure 9 shows the rate kernels derived from shape evolution in Figure 7.

It may be difficult to obtain a numerical solution to the population balance eq 36 due to following reasons. A corner or edge of a crystal has an infinite curvature, which decreases with dissolution and approaches a very small value for a flat surface. In this process of corner transforming to a flat face, the curvature has spanned the entire positive real axis which is impossible to track numerically. An approximation can be made to define a maximum value of curvature. For example, a crystal of unit size whose corner has a curvature of 100 (equivalently, the radius of curvature is 100 times smaller than the dimension of crystal) will still look like a corner on a relative scale. In other words, morphologies of crystals with sharp corners or corners

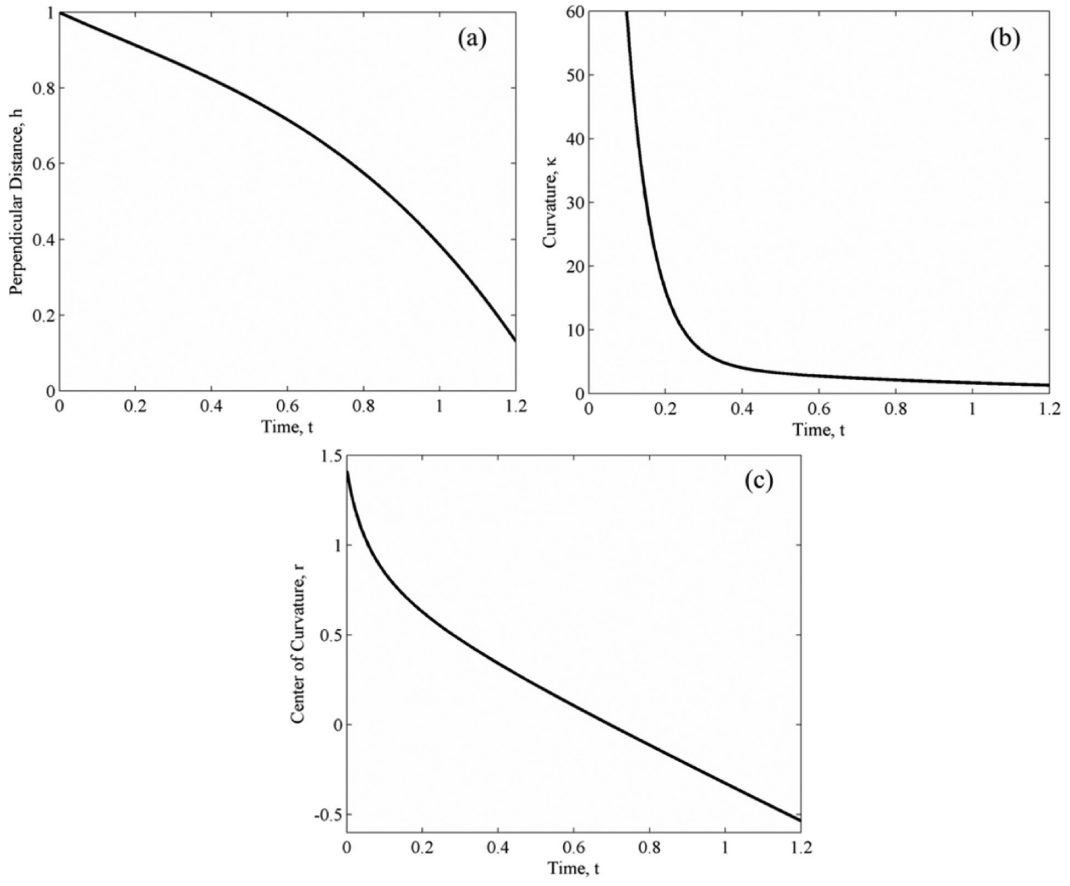

Figure 8. Evolution of (a) perpendicular distances of F-faces, (b) curvatures at the corners, and (c) the center of curvatures in Figure 7.

dx.doi.org/10.1021/cg500939t | Cryst. Growth Des. 2014, 14, 5647−5661

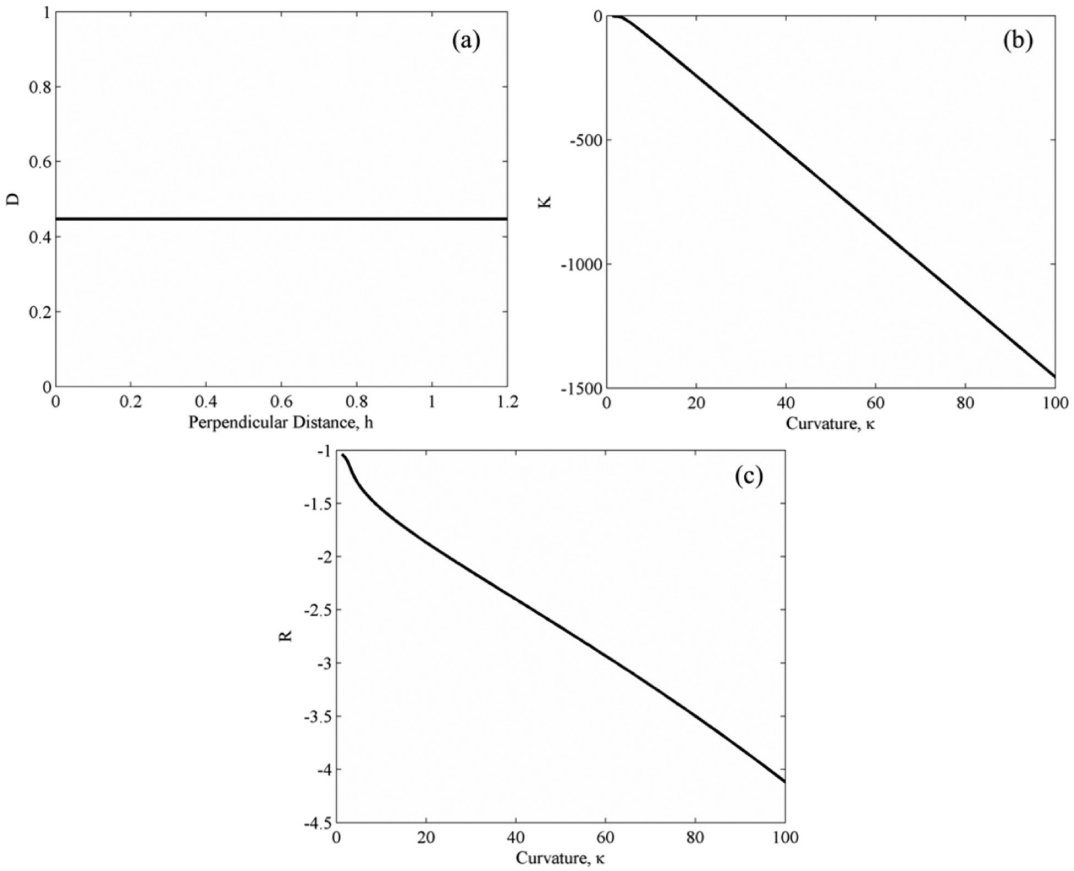

Figure 9. Rate of change of (a) perpendicular distance (D), (b) curvature (K), and (c) the center of curvature (R).

with a curvature value of 100 are almost identical. Similarly, the center of curvatures starting from the corner of crystal can span the entire negative real axis as it progresses toward a flat face. As the curvature in Figure 8b decreases to a value of 1, the curved corner surface in Figure 7 becomes more flat. Here the center of curvature at a distance of −0.5 from origin yields an almost flat surface. Such analysis can provide bounds on the values of curvature and its center to obtain a numerical solution. The analysis presented here uses a set of perpendicular distance, curvature, and its center to describe dissolution of a crystal with one family of faces. A real crystal with multiple families of faces will require multiple sets of internal coordinates.

3. IDENTIFICATION OF POLAR PLOTS

Section 2 discusses the dynamics of crystal morphology due to the associated polar plots of growth rates and dissolution rates for different governing mechanisms. The polar plots are the function of crystal structure and the environmental conditions. The fate of crystal morphology is determined by the polar plots. Therefore, it is crucial to predetermine polar plots to predict morphological properties of crystalline materials for different applications. The subsequent section will present a methodology to compute polar plots from the dynamic information on crystal morphology.

3.1. Solution of the Characteristics. The characteristics for the evolution of surface $\varphi(\mathbf{r};t) = 0$ along the normal vector $\mathbf{n}$ is given as

$$\mathbf{n}\cdot\frac{d\mathbf{r}}{dt} = v(\mathbf{n}) \tag{37}$$

where $v(\mathbf{n})$ is equal to $G(\mathbf{n})$ for growth and $-D(\mathbf{n})$ for dissolution. The objective here is to calculate $v(\mathbf{n})$ from the dynamic data on $\varphi(\mathbf{r};t) = 0$. The *in situ* experiments, as discussed in Sections 4 and 5, on crystal growth or dissolution using hot-stage microscopy can provide the dynamic data on surface evolution. The transient images of crystals provide information on $\varphi(\mathbf{r};t) = 0$ for discrete values of $\mathbf{r}$ and t. Therefore, it is reasonable to discretize eq 37 to calculate the polar function, such as

$$v_{i,j}(\mathbf{n}_i) = \mathbf{n}_i\cdot\frac{\mathbf{r}_i(t_j) - \mathbf{r}_i(t_{j+1})}{t_j - t_{j+1}},\ i = 1, 2, ..., N_\theta;\ j = 1, 2, ..., N_T \tag{38}$$

where $v_{i,j}$ is the speed of the position vector $\mathbf{r}_i$ along the surface normal $\mathbf{n}_i$ at time t_j. Here the time derivative is evaluated at t_j using forward-difference scheme which is accurate to the order of Δt. Other schemes of higher order accuracy to discretize first order derivatives can also be used in 38. Since the surface normal does not change along the characteristics, the position vectors $\mathbf{r}_i(t_j)$ on $\varphi(\mathbf{r};t_j) = 0$ and $\mathbf{r}_i(t_{j+1})$ on $\varphi(\mathbf{r};t_{j+1}) = 0$ must be chosen such that

$$\nabla\varphi(\mathbf{r}_i(t_j);\ t_j) = \nabla\varphi(\mathbf{r}_i(t_{j+1});\ t_{j+1}) \tag{39}$$

Experimentally determined velocities of faces at fixed operating conditions can show variation with time, which can be considered as random,[28] and hence they can averaged as,

$$v_i(\mathbf{n}_i) = \frac{1}{N_T}\sum_{j=1}^{N_T} v_{i,j}(\mathbf{n}_i),\ \ i = 1, 2, ..., N_\theta \tag{40}$$

dx.doi.org/10.1021/cg500939t | Cryst. Growth Des. 2014, 14, 5647−5661

The growing or dissolving crystals will drive the solution toward the saturation limit, which will reduce their face-specific velocities. To compensate for the effect of changing supersaturation or subsaturation on the measured face-specific velocities, eq 40 can be written as the weighted sum. Appendix I shows the formulation to obtain such a weighted sum.

The measured polar plots may also lack crystal symmetry due to spatial inhomogeneity in experimental conditions. The polar plots must retain the symmetry of crystal, so that

$$v_i(\mathbf{R}_1\mathbf{n}_i) = v_i(\mathbf{R}_2\mathbf{n}_i) = ... = v_i(\mathbf{R}_S\mathbf{n}_i) \tag{41}$$

where $\mathbf{R}_1$, $\mathbf{R}_2$, ..., $\mathbf{R}_s$ are the rotation matrices identified from the crystal symmetry such that $\mathbf{R}_1\mathbf{n}_i$, $\mathbf{R}_2\mathbf{n}_i$, ..., $\mathbf{R}_S\mathbf{n}_i$ belong to the same family. The crystal symmetry can be enforced to the polar plots in the following way

$$v_i(\mathbf{n}_i) = \frac{1}{S}\sum_{j=1}^{S} v_i(\mathbf{R}_j\mathbf{n}_i) \tag{42}$$

3.2. Numerical Procedure: Moving Tangent Method.

One of the reliable experimental techniques to measure dynamical changes in crystal morphologies is microscopic imaging. The quality and number of time lapse images determine the quality of the measured polar plots. In the following, we have discussed a numerical procedure based on the moving tangent method to determine polar plots from dynamic images of 2D crystals.

Step 1: The standard image processing and segmentation algorithms can yield the contour of the 2D crystal for each time-lapsed image. The resolution of the images can be used to determine the position coordinates of each pixel in the contour.

Step 2: N_T is equal to the number of time-lapse images. The upper limit on N_θ is determined from the number of pixels forming the smallest contour. Such a selection will ensure that the number of normal vectors does not exceed the number of pixels. Moreover, the selection of N_θ must comply with the crystal symmetry such that all $\mathbf{R}_j\mathbf{n}_i$ belong to the set $\{\mathbf{n}_1, \mathbf{n}_2, ..., \mathbf{n}_{N_\theta}\}$. For example, if the crystal has 4-fold symmetry then N_θ must be an integer multiple of four.

Step 3: The number of pixels can exceed N_θ for larger contours. Therefore, we need to identify only those pixels which best describe the surface normals $\{\mathbf{n}_1, \mathbf{n}_2, ..., \mathbf{n}_{N_\theta}\}$. We define a compact notation $\mathbf{r}_{i,j} \equiv \mathbf{r}_i(t_j)$ which represents position vector of a pixel with surface normal $\mathbf{n}_i$ on the jth contour. The labeled pixels $\mathbf{r}_{i,j}$ are the points where planes with normal $\mathbf{n}_i$ touches $\varphi(\mathbf{r}_i;t_j) = 0$, such that they have maximum perpendicular distances from the origin.

$$\max_{\mathbf{r}_{i,j}}(\mathbf{n}_i^T\mathbf{r}_{i,j}) \tag{43}$$

Graphically, the points $\{\mathbf{r}_{i,1}, \mathbf{r}_{i,2}, ..., \mathbf{r}_{i,N_T}\}$ can be obtained by moving the tangent plane with normal vector $\mathbf{n}_i$ over all other contours.

Step 4: Use eqs 38, 40, and 42 to determine the polar plot $v_i(\mathbf{n}_i)$.

4. MATERIALS AND METHODS

The experiments on the dissolution of single crystal of succinic acid were done in a crystallization cup using hot-stage optical microscopy. A saturated solution of succinic acid (Sigma-Aldrich, > 99% purity) in water was prepared at 40 °C, and the solution was slowly cooled down to 28 °C, which yielded nicely shaped crystals. A single crystal of succinic acid was carefully transferred to the (1 cm × 1 cm) crystallization cup containing saturated solution of succinic acid at 28 °C. After the crystal settled down, the saturated solution was filled up to the brim of the crystallization cup, which was then covered with glass slip and sealed with grease. Alternatively, crystals can be grown inside the crystallization cup by cooling down the saturated solution. Figure 10 shows the crystallization cup assembly. The size of the crystal shown is much larger than what is used in the study.

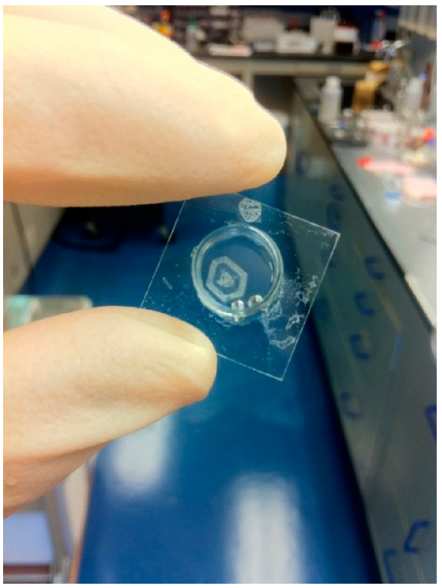

Figure 10. Crystallization cup assembly containing succinic acid crystal in saturated solution. The crystallization cup is covered with coverslip and made leak proof by sealing with high vacuum grease.

The crystallization cup assembly was transferred to the hot-stage setup (Linkam, LTS350) on the optical microscope (Nikon, Elipse LV100POL). The complete setup for conducting in situ dissolution is shown in Figure 11. With the knowledge of the solubility of succinic acid in water, a known amount of subsaturation can be created by quickly raising the temperature and maintaining it to a specific value using the temperature controller of the hot-stage. The experiments were conducted at constant temperatures such as 31, 33, 38, 43, and 48 °C. The dissolution of succinic acid crystal was recorded by taking time-lapsed images.

Figure 11. Hot-stage optical microscope with crystallization cup.

5. RESULTS AND DISCUSSION

The micrographs were processed in a similar way as shown by Singh et al.[29] to identify contours of crystals. Figure 12 demonstrates the sequential processes involved in obtaining contour from the micrograph.

dx.doi.org/10.1021/cg500939t | Cryst. Growth Des. 2014, 14, 5647−5661

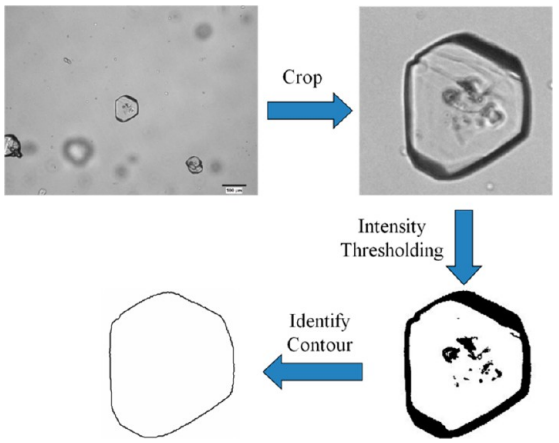

Figure 12. Image processing and segmentation to obtain contour of succinic acid crystal.

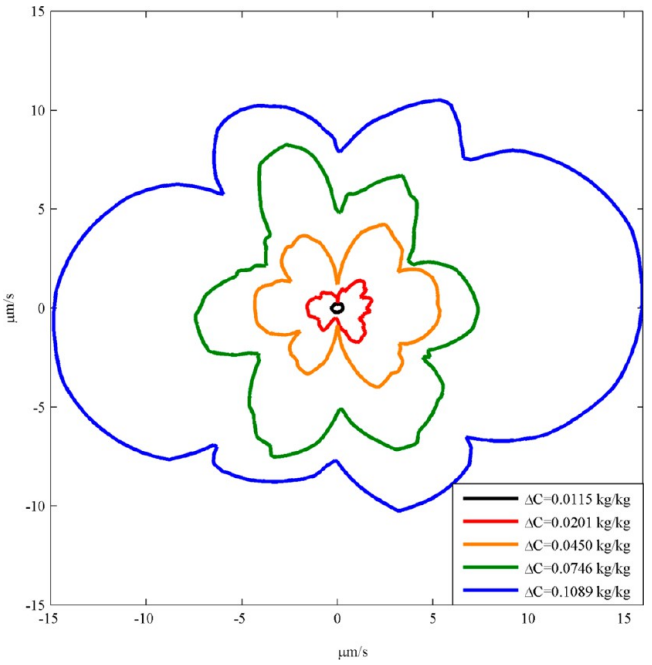

Figure 13. Measured polar plots of dissolution rates of succinic acid at different subsaturations.

The sequence of time-lapsed images can be processed to obtain contours of crystals. The moving tangent method was used to obtain polar plots of dissolution rates. Figure 13 shows the measured polar plots for different subsaturations and a fixed temperature of 28 °C. The size of crystal does not change much in the first few seconds of dissolution, which ensures constant subsaturation. However, the degree of subsaturation will decrease as the crystal dissolves. Therefore, the time-lapsed images recorded in the beginning of dissolution experiments are used to obtain the polar plots. These polar plots are aligned such that north and south directions correspond to {010} faces. The size of the polar plots increases with the degree of subsaturation. The minima of the polar plots correspond to the F-faces of succinic acid such as {010} and {110}. Clearly, the polar plots are irregular and lack symmetry of succinic acid crystal. Such irregularities can be due to diffusional inhomogeneity in the crystallization cup causing nonuniform subsaturations around the crystal. One of the ways to remove such noise from the as-measured polar plots is by enforcing crystal symmetry. The morphologies predicted from the as-measured and symmetry-applied polar plots will be different. Also, the random behavior of polar plots will prevent crystals from attaining steady states.

The succinic acid crystal has 2-fold symmetry and a mirror plane along the (010) direction. The symmetry can be applied according to eq 42 to obtain symmetric polar plots. Figure 14 shows the polar plot of dissolution rates (at ΔC = 0.0746 kg/kg) before and after applying symmetry. The symmetry-applied polar plot shows distinct minima and maxima corresponding to the slowest and fastest dissolving faces.

6. CONCLUSIONS

This article revisits the existing surface evolution theory for crystal growth and dissolution to provide more insights into the development of steady-state morphologies. The appearances of fans and shocks on a circular crystal due to growth/dissolution were studied for different limiting mechanisms such as surface integration/disintegration, surface diffusion, and bulk diffusion. The steady-state morphologies obtained from the Wulff construction are usually faceted for diffusion-free growth, which is due to the presence of cusps in the polar plots. The independent growth characteristics emanating from the circular crystal tend to intersect to produce propagating shocks. Although the trajectories of shocks depend on the initial morphology, their final locations are dependent only on the fans participating in the steady-state morphology. The fans on growth morphologies appear due to bifurcation (in case of 2D crystals) or multifurcation (in the case of 3D crystals) of propagating shocks. The characteristics satisfying conditions 9 and 10 will contribute to shocks and fans, respectively, and the rest will produce curved interfaces. The surface integration limited growth of crystals often leads to fully faceted morphology, whose characteristics can be lumped according to eq 13 to describe shape evolution using perpendicular distances. The faceted morphologies can also undergo various transformations based on relative growth rates, which can be determined by construction morphology domain. As the vertices and edges of a faceted morphology can grow much faster than the corresponding flat faces, they can be influenced by diffusion limitations. Under such conditions, the steady-state growth morphologies can have more rounded corners and edges with either constant or varying curvature based on the governing mechanism being bulk diffusion limited or surface diffusion limited, respectively. One of the distinguishing features of growth morphologies is that they can always attain the steady state at fixed growth rates.

The possible steady-state dissolution morphology can be determined from the Wulff construction on the corresponding slowness surface given in eq 18. Unlike growth morphologies, the dissolution morphologies may not always attain steady state. Since the slowness surface is the inverse of the polar function of dissolution rates, the steady-state morphology is composed of fastest-dissolving faces. The mechanism of the appearances of fans and shocks in dissolution morphologies are completely different than that of growth morphologies. The fans appear along the surface normal corresponding to the maxima of the polar plots of dissolution rates, which is due to the flattening of curvature on the initial morphology. The curvature reduces because the characteristics diverge away from the location of the maxima and gravitate toward the location of

dx.doi.org/10.1021/cg500939t | Cryst. Growth Des. 2014, 14, 5647−5661

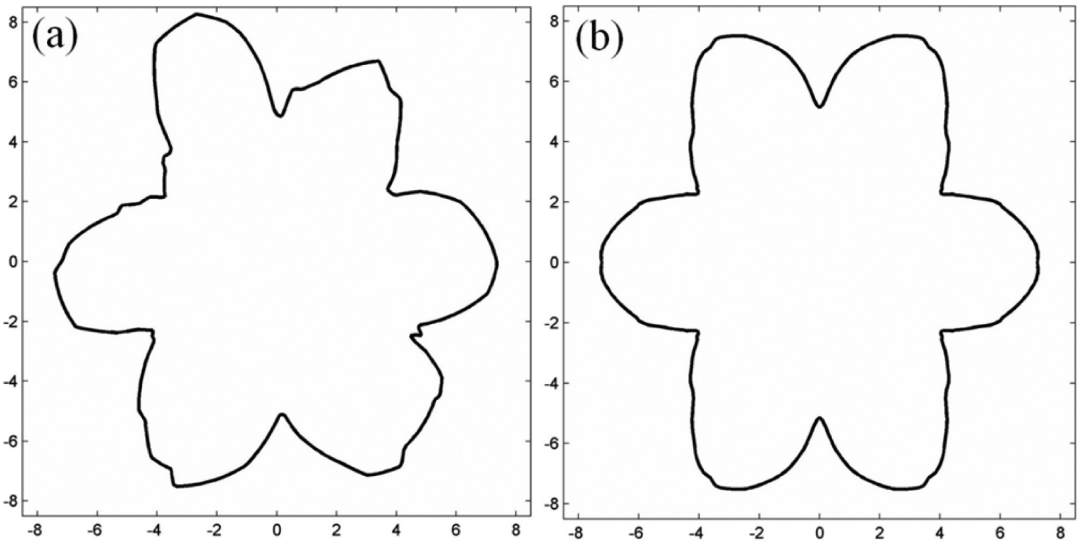

Figure 14. Polar plot of dissolution rates (a) before applying symmetry and (b) after applying symmetry.

minima, where they intersect to form propagating shocks. The trajectories of shocks are dependent on the initial morphology, whereas their locations on steady-state morphology only depend on the relative positions of fans. The steady morphologies for growth or dissolution can be completely smooth if the growth or dissolution of entire crystal is governed by diffusion limitations. The steady-state dissolution morphology can be attained if (1) the constituting faces belong to same family or (2) relative perpendicular distances of the constituting faces on the initial morphology are proportional to the corresponding relative dissolution rates.

The alternating operations of growth and dissolution offer great prospects to control crystal morphologies and related properties. The curved interfaces on crystal morphologies are inevitable when switching between growth and dissolution. We have shown an efficient way for accounting the evolution of curved interfaces by deriving kinetic equations for the corresponding curvatures. The evolution of a convex crystal can be completely described by the kinetic equations for perpendicular distances, curvatures, and their centers, thus providing an efficient framework to describe morphology distributions using population balance equations.

This article also presents a moving tangent method to experimentally measure polar plots of dissolution rates using time-lapse images obtained from hot-stage microscopy. The methodology involves (1) image processing of time-lapse images to obtain contours of crystals, (2) selecting appropriate N_θ and N_T, (3) assigning labels to the pixels on each contour using moving tangent method, and (4) computing polar plots of dissolution rates and applying crystal symmetry. The methodology was implemented to measure polar plots of dissolution rates of succinic acid at different subsaturations and fixed temperature. The polar plots expand in size with an increase in the degree of subsaturation. The measured polar plots show six distinct minima corresponding to the F-faces of succinic acid crystal. The irregularity in the measured polar plots can be due to inhomogeneous subsaturations in the crystallizer. Prior information on the source of inhomogeneity in the crystallizer along with the crystal symmetry can be used to obtain smooth polar plots. The morphology predicted from the smoothened polar plots will depend on the underlying assumptions of the smoothening operation. In this case, crystal symmetry alone provides an excellent basis for the smoothing operation. The current methodology also can be extended to obtain polar plots of growth rates using hot-stage microscopy. A three-dimensional measurement of polar plots will require either an instrument with in-depth resolution (such as confocal or X-ray microscopes)[29] or an advanced technique to deconvolute the 3D shape from a 2D image.[30] This work has presented a methodology for rapid measurement of polar plots when the time-lapse images of crystals are available.

APPENDIX I: INVERSE-PROBLEM FORMULATION TO MEASURE FACE-SPECIFIC VELOCITIES

The discretized form 38 of the characteristics 37 can be rewritten in a matrix form as

$$\mathbf{v}_i = \dot{\mathbf{R}}_i \mathbf{n}_i, \quad i = 1, 2, \ldots, N_\theta \tag{44}$$

where $\mathbf{v}_i$ is a column vector of speeds of ith face at N_T time intervals and $\dot{\mathbf{R}}_i$ is a matrix with row vectors representing change in position vector in jth time interval. The residual of eq 44 can be written as

$$\delta_i = [\mathbf{v}_i - \dot{\mathbf{R}}_i \mathbf{n}_i]^T [\mathbf{v}_i - \dot{\mathbf{R}}_i \mathbf{n}_i] + \lambda \mathbf{v}_i^T \mathbf{A}^T \mathbf{A} \mathbf{v}_i \tag{45}$$

where λ is a Tikhonov regularization parameter and $\mathbf{A}$ is a diagonal matrix accounting for the experimental errors. Minimization of the residual yields

$$\mathbf{v}_i = [\mathbf{I} + \lambda \mathbf{A}]^{-1} \dot{\mathbf{R}}_i \mathbf{n}_i \tag{46}$$

The average value of the components of $\mathbf{v}_i$ would give the required equation,

$$v_i(\mathbf{n}_i) = \frac{1}{N_T} \sum_{j=1}^{N_T} \frac{v_{i,j}(\mathbf{n}_i)}{1 + \lambda A_i}, \quad i = 1, 2, \ldots, N_\theta \tag{47}$$

Equation 40 must be replaced with 47 when experimental errors are quantifiable.

AUTHOR INFORMATION

Corresponding Author

*E-mail: ramkrish@purdue.edu. Tel: (765) 494-4066.

Funding

The authors (M.R.S. and D.R.) gratefully acknowledge the funding support from GPRD-Process Engineering department

of AbbVie Inc., North Chicago. M.R.S also acknowledges McDonnell Douglas Fellowship administered through Purdue College of Engineering to support this research.

Notes

The authors declare no competing financial interest.

LIST OF SYMBOLS

$\mathbf{c}$	vector of crystallization conditions
D	absolute dissolution rate of crystal face along vector $\mathbf{n}$ [m s^{-1}]
$\mathbf{D}$	m-dimensional vector of dissolution rates corresponding to m crystal faces [m s^{-1}]
f	scalar function of face-specific normals $\mathbf{n}$
G	absolute growth rate of crystal face along vector $\mathbf{n}$ [m s^{-1}]
$\mathbf{G}$	m-dimensional vector of growth rates corresponding to m crystal faces [m s^{-1}]
h_i	perpendicular distance of faces in ith family [m]
$\tilde{h}_i$	perpendicular distance of ith face [m]
$\mathbf{h}$	m-dimensional vector of perpendicular distances of faces belonging to m families [m]
K	rate of change of curvature [m^{-1} s^{-1}]
m	total number of families of faces [−]
$n(h,\kappa,r;t)$	number density in crystal state space [m^{-4}]
$\mathbf{n}$	surface normal vector [−]
N_T	total number of time-lapsed images [−]
N_θ	total number of normal vectors [−]
P	arbitrary surface property
$\mathbf{r}$	three-dimensional position vector [m]
R	rate of change of the center of curvature [m s^{-1}]
$\mathbf{R}$	rotation matrices [−]
s	arc length on a crystal surface [m]
S	total number of symmetry operations [−]
t	crystallization time [s]
$\mathbf{T}$	surface tangent vector [−]
v	speed of crystal face along normal $\mathbf{n}$ [m s^{-1}]
α_{ij}	geometric dependence corresponding to appearance or disappearance of the ith family on the jth family [−]
κ	curvature of crystal surface along tangent $\mathbf{T}$ [m^{-1}]
φ	crystal surface [−]
φ_0	initial crystal surface [−]
τ	slowness or inverse of face-specific dissolution rates [s m^{-1}]
θ	angle between two surface normals [−]
ζ	scalar function of crystal surface φ [m^{-2}]

REFERENCES

(1) Herring, C. The use of classical macroscopic concepts in surface energy problems. In *Structure and Properties of Solid Surfaces*; Gomer, R.; Smith, C. S., Eds.; University of Chicago Press: Chicago, 1953; pp 5−72.

(2) Wulff, G. Zur Frage der Geschwindigkeit des Wachstums und der Auflosung der Krystallflachen. *Z. Krystallogr. Mineral.* **1901**, *34*, 449.

(3) Gibbs, J. W. On the equilibrium of heterogeneous substances. *Trans. Connecticut Acad. Arts Sci.* **1878**, *3*, 343−524.

(4) Taylor, J. E. Crystalline variational problems. *Bull. Am. Math. Soc.* **1978**, *84* (4), 568−588.

(5) Hartman, P.; Perdok, W. On the relations between structure and morphology of crystals. I. *Acta Crystallogr.* **1955**, *8* (1), 49−52.

(6) Hartman, P.; Perdok, W. On the relations between structure and morphology of crystals. II. *Acta Crystallogr.* **1955**, *8* (9), 521−524.

(7) Hartman, P.; Perdok, W. On the relations between structure and morphology of crystals. III. *Acta Crystallogr.* **1955**, *8* (9), 525−529.

(8) Cahn, J.; Taylor, J.; Handwerker, C. Evolving crystal forms: Frank's characteristics revisited. *Sir Charles Frank, OBE, ERS: An Eightieth Birthday Tribute*; Chambers, R. G. et al., Ed.; Adam Hilger: New York, 1991; pp 88−118.

(9) Taylor, J. E.; Cahn, J. W.; Handwerker, C. A. Geometric models of crystal growth. *Acta Metall. Mater.* **1992**, *40* (7), 1443−1474.

(10) Frank, F. On the kinematic theory of crystal growth and dissolution processes. In *Growth and Perfection of Crystals*; Doremus, R. H.; Roberts, B. W.; Turnbull, D., Eds.; Wiley: New York, 1958; pp 411−419.

(11) Lighthill, M.; Whitham, G. On kinematic waves. I. Flood movement in long rivers. *Proc. R. Soc. London A* **1955**, *229* (1178), 281−316.

(12) Lighthill, M. J.; Whitham, G. B. On kinematic waves. II. A theory of traffic flow on long crowded roads. *Proc. R. Soc. London A* **1955**, *229* (1178), 317−345.

(13) Lacmann, R.; Franke, W.; Heimann, R. The dissolution forms of single crystal spheres: I. Theory for the molecular-kinetics interpretation. *J. Cryst. Growth* **1974**, *26* (1), 107−116.

(14) Shaw, D. W. Morphology analysis in localized crystal growth and dissolution. *J. Cryst. Growth* **1979**, *47* (4), 509−517.

(15) Tellier, C. Etching of semiconductor cubic crystals: Determination of the dissolution slowness surfaces. *J. Cryst. Growth* **1990**, *100* (3), 515−526.

(16) Brahim-Bounab, A.; Amaudrut, J.; Tellier, C. Dissolution slowness surfaces of cubic crystals. *J. Mater. Sci.* **1991**, *26* (20), 5585−5594.

(17) Beregi, E.; Sterk, E.; Tanos, F.; Hartmann, E.; Lábár, J. The dissolution forms of YIG single crystal spheres. *J. Cryst. Growth* **1983**, *65* (1), 562−567.

(18) Heimann, R.; Franke, W.; Lacmann, R. The dissolution forms of single crystal spheres: IV. Dissolution of MgO. *J. Cryst. Growth* **1975**, *28* (1), 151−156.

(19) Snyder, R. C.; Doherty, M. F. Faceted crystal shape evolution during dissolution or growth. *AIChE J.* **2007**, *53* (5), 1337−1348.

(20) Snyder, R. C.; Studener, S.; Doherty, M. F. Manipulation of crystal shape by cycles of growth and dissolution. *AIChE J.* **2007**, *53* (6), 1510−1517.

(21) Snyder, R. C.; Veesler, S.; Doherty, M. F. The evolution of crystal shape during dissolution: predictions and experiments. *Cryst. Growth Des.* **2008**, *8* (4), 1100−1101.

(22) Osher, S.; Sethian, J. A. Fronts propagating with curvature-dependent speed: algorithms based on Hamilton-Jacobi formulations. *J. Comput. Phys.* **1988**, *79* (1), 12−49.

(23) Winn, D.; Doherty, M. F. Modeling crystal shapes of organic materials grown from solution. *AIChE J.* **2000**, *46* (7), 1348−1367.

(24) Singh, M. R.; Verma, P.; Tung, H.-H.; Bordawekar, S.; Ramkrishna, D. Screening Crystal Morphologies from Crystal Structure. *Cryst. Growth Des.* **2012**, *13* (4), 1390−1396.

(25) Singh, M. R.; Ramkrishna, D. A Comprehensive Approach to Predicting Crystal Morphology Distributions with Population Balances. *Cryst. Growth Des.* **2013**, *13* (4), 1397−1411.

(26) Ramkrishna, D. *Population Balances: Theory and Applications to Particulate Systems in Engineering*; Academic Press: New York, 2000.

(27) Ramkrishna, D.; Singh, M. R. Population Balance Modeling: Current Status and Future Prospects. *Annu. Rev. Chem. Biomol. Eng.* **2014**, *5* (1), 123−146.

(28) Singh, M. R.; Ramkrishna, D. Dispersions in crystal nucleation and growth rates: Implications of fluctuation in supersaturation. *Chem. Eng. Sci.* **2014**, *107*, 102−113.

(29) Singh, M. R.; Chakraborty, J.; Nere, N.; Tung, H. H.; Bordawekar, S.; Ramkrishna, D. Image-Analysis-Based Method for 3D Crystal Morphology Measurement and Polymorph Identification Using Confocal Microscopy. *Cryst. Growth Des.* **2012**, *12* (7), 3735−3748.

(30) Borchert, C.; Sundmacher, K. Morphology evolution of crystal populations: Modeling and observation analysis. *Chem. Eng. Sci.* **2012**, *70*, 87−98.